Second Interim Progress Report
**Monitoring Active Region Development on the Far Side of the Sun**

| | |
|---|---|
| NOAA SBIR Project # | WC 133R-15-CN-0076 |
| PI | C. Lindsey (NWRA) |
| Co-Is | D.C. Braun, K.D. Leka, G. Barnes & J. Werne (NWRA);<br>P. Liewer (JPL);<br>P. Scherrer & J. Zhao (Stanford); and<br>F. Hill & T. Wentzel (NSO/GONG) |
| Period of Performance | November 16, 2015–January 15, 2016 |
| Date | January 22, 2016 |

## 1. Review

This Report covers the second two months, i.e., "Period 2," of the Phase-1 component of a Project whose purpose is to develop seismic monitoring of the Sun's far hemisphere to address needs of general space-weather forecasting. The particular need in question is that of detecting and monitoring active regions in the Sun's far hemisphere, particularly magnetic flux that has emerged in the far hemisphere unobserved by direct electromagnetic monitoring. The first report, summarizing Period 1 of the project, focused on the question of the reliability of helioseismic maps of active regions on concurrent EUV observations by NASA's Solar TErrestrial Relations Observatory (STEREO). These maps are computed from SDO/HMI and GONG helioseismic observations, and are published by Stanford's Joint Science Operations Center (JSOC) and the National Solar Observatory (NSO). The stronger signatures that appear in these maps are recognized by Stanford's Far-Side Seismic Solar Monitor (FSSSM) as indicative of probable "large active regions."

The main focus of the First Report was the reliability of the FSSSM large-active-region signatures. Our study found them to be a highly reliable indicator of conspicuous EUV sources, particularly those in HeI 304 Å, and that these signatures appeared within approximately a degree or two of arc over the Sun's surface of the centroids of their seismic signatures. However, we found a nearly equal number of significant, generally weaker EUV sources whose seismic signatures never broke the FSSSM threshold for large-active-region status. Many of these were beneath the noise level of the seismic monitor—meaning the seismic signatures not only failed to qualify as "large," but also never reached the practical threshold for detection. This is consistent with the seismic monitor being less sensitive than diagnostics based upon directly observed electromagnetic radiation—the statistical weight of 300-second oscillations integrated over a period of days is no match for that of the femtosecond-period oscillations of visible light, even over a single millisecond of the latter. Nevertheless, the FSSSM can clearly see lare active regions space-weather forecasters would want to know about. The practical role for seismic mapping of the Sun's far hemisphere could be its utility (1) as a complement to

STEREO early into the time frame for a Phase-3 implementation, when coverage of the Sun's far hemisphere by the combined STEREOs will begin to diminish, and/or (2) that of a back-up should we lose one or more of the STEREOs.

The object of Period 2 has been a more quantitative assessment of what seismic signatures can tell us about the regions that elicit them than was attempted in Phase 1. There are now two domains of inquiry:

(1) the quantitative relationship between the "strengths," $S$, of seismic signatures as gauged by the Stanford seismic monitor and the EUV intensities, $J$ (Mihalas 1978), of regions associated with them; and

(2) the quantitative relationship between $S$ and attributes of the distribution of magnetic-flux that characterizes the regions. The present focus is the "unsigned magnetic flux," $\Phi$, that appears in the neighborhood of a seismic signature when its location subsequently rotates into direct view from Earth.

In addition to these objectives we also pursue the development of basic analytical tools to characterize the morphologies of helioseismic signatures for eventual applications in modeling the distributions of newly emerged magnetic flux.

A summary of project tasks from the original Phase-1 Proposal follows:

1. Compute and assimilate far-side maps for analysis.

2. Develop an algorithm to identify individual signatures attributed to active regions in seismic maps of the Sun's far hemisphere.

3. Evaluate uncertainties in the existence of far-side magnetic regions to which seismic signatures are attributed.

4. Quantitatively evaluate errors in the locations attributed to far-side active regions by seismic signatures.

5. Evaluate uncertainties in the strengths and growth rates of seismic signatures attributed to far-side active regions.

6. Determine the long-term reliability of seismic signatures as characteristic of active-regions.

7. Deliver reports, prototype code and documentation of the Project, and hold meetings to discuss Project results.

An update of the graphic representation of the schedule of the workplan is presented here:

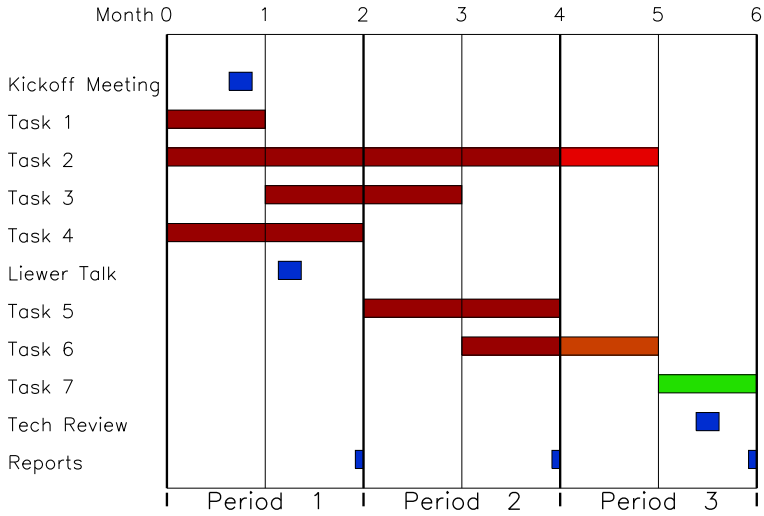


The main change in the work plan stated in the First Report is the extension of Task 2. This is described in §4 of this report. This was developed in Period 1 sufficiently to proceed with all other tasks of the project. However, looking toward a Phase-2 project, further development is desired, and is proceeding accordingly.

## 2. Quantitative Characterization of Seismic Signatures of Activity in the Sun's Far Hemisphere

The primary object of the First Report was to address the question of the reliability of the FSSSM large-active-region discriminator as an indicator of significant EUV sources as observed concurrently by STEREO. For this study, CoI Liewer compared all of the FSSSM large-active-region signatures from February through June of 2011 (Interval 1, 12 seismic signatures in all) and from January through April of 2012 (Interval 2, 10 more signatures) with concurrent STEREO maps of HeI 304 Å intensity. As noted in §1, she found that all of the seismic signatures were cospatial with conspicuous STEREO sources, notwithstanding the existence of HeI 304 Å sources clearly visible to STEREO whose seismic signatures were less clear or insignificant. The statistics were based on essentially single-bit, i.e., "yes/no," evaluations of whether a single significant seismic signature was matched by a single significant EUV source, with no further indication of what finer detail the seismic signature might indicate about the EUV source.

The object of our Period-2 effort has been to examine quantitatively the relationship between the strengths of the helioseismic signatures and quantitative aspects of the physical attributes of the active region indicated. We are now ready to describe in some detail the two major aspects of solar activity whose relationship to helioseismic signatures are the focus of this study:

(1) the concurrently observed intensity, $J$ (Mihalas 1978), of the region in HeI 304 Å radiation as determined by STEREO maps, and

(2) the unsigned magnetic flux, $\Phi$, through the same as determined by HMI magnetic maps.

We begin with two analyses of just the seismic signatures with no reference to $J$ and $\Phi$ as a gauge for the kinds of day-to-day variations the seismic signatures show, whether as a result of measurement uncertainties or of how the active regions themselves may vary during their transit of the far hemisphere. The seismic maps express the phase shift, $\Delta\phi$, for each point in the Sun's far hemisphere, of a cross-correlation between seismic waves impinging into said point and its returning echo. For this discussion, the "strength," $S$, of a seismic signature is defined as

$$S(\mathcal{R}) \;=\; \frac{1}{2\pi}\int_{\mathcal{R}} \Delta\phi \; d^2a, \tag{1}$$

where $\Delta\phi$ is the phase shift in the foregoing correlation, $da$ represents the differential elements of area on the Sun's surface over which the seismic signature extends, and $\mathcal{R}$ is a region enclosing the signature. The FSSSM assigns designations to the signatures it identifies as large active regions. The locations and strengths of these are tabulated twice daily on `http://jsoc.stanford.edu/data/farside/AR_Lists`, the strengths being expressed in units of $\mu$hem radians.

### *2.1 Evaluation of Relative Sensitivities of Seismic Maps Computed from HMI and GONG Observations*

CoI Frank Hill employed histograms of the strengths of GONG and HMI seismic signatures with and without the presence of solar activity in the far hemisphere, and cotemporal scatter plots comparing the two for clues as of the random uncertainties due to "realization noise" in far-side seismic signatures.[†] Only a brief summary of CoI Hill's study is presented here. The full study is posted on `www.cora.nwra.com/~lindsey/fhill_errors_study.pdf`. CoI Hill's study is based on comparisons of far-hemispheric seismic maps computed from HMI and GONG observations. These maps were made with the seismic algorithm developed for GONG++ between 2000 and 2002, applied to both GONG and HMI seismic observations, as distinguished from the more recent, improved (we think) algorithm applied to HMI maps

[†] In the usual context of solar seismology, "realization noise" refers to uncertainties associated with oscillatory signatures that result from limitations in the observations even when the instrumental noise is nil. For example, we understand that the power spectrum of a time series of Gaussian random values is statistically flat. However, when we compute the Fourier transform of such a time series and plot the square of its modulus, the result is invariably a spectrum that is far from flat, and in fact, is fully as stochastic in frequency as the square of the original time series is in time. Realization noise refers to the difference between the mean power spectrum averaged a finite ensemble and the ideal case of an infinite ensemble—whether the resulting spectrum is flat or otherwise. Optical imaging both in the seismic and electromagnetic spectra is subject to realization noise in ways highly analogous to those which apply to power spectra.

and published by Stanford. Hill made independent histograms of the distributions of the seismic signatures from both of these data sets with and without active-region signatures in the domain of analysis. He also plotted the mean, variance, skewness and kurtosis of each, noting a strong sensitivity of the skewness and kurtosis (and even more so, their product) to the presence of activity.

CoI Hill also made cospatial scatter plots of helioseismic maps of the far hemisphere, both in the quiet Sun and in active regions. Datapoints representing magnetic regions were clearly distinct from those of the non- or weakly-magnetic regions. The scatter plots show a Pearson cross-correlation coefficient, $P$, of $\sim$0.6 for the quiet Sun, suggesting that realization noise is a significant component, but not necessarily the entirety of both signatures, i.e., instrumental noise could be significant. In active regions, $P$ is of order 0.85, with a relative slope, $S_{GONG}/S_{\rm HMI}$ of $\sim$1, indicating approximately equal sensitivities of the GONG and HMI maps. The scatter width in the HMI maps is $\sim$1.4 times that of the GONG scatter width, implying greater noise in the former. However, this appear to be inherent in the HMI maps having a somewhat finer spatial resolution than the GONG maps.

The scatter plots also show anomalous clusters of points, "mystery regions," that are significantly offset from the main centroids representing most of the quiet Sun and magnetic regions. The primary mystery regions appears to represent the equatorial band (approximately $\pm 10^\circ$ latitude) between active regions, within which HMI maps show negative seismic signatures and GONG maps show positive signatures. This may be the result of differing corrections for the effects on GONG far-side seismic signatures of magnetic regions in the near hemisphere than for HMI far-side seismic signatures—a systematic error that can, in principle, be equalized between the HMI and GONG algorithms, if not corrected altogether.

### *2.2 Temporal Variability of HMI Active-Region Signatures in Seismic Maps Computed with the New Seismic Algorithm, and the Potential for Assessing Growth Rates*

A realistic assessment of the growth rates of strengths, $S$, of seismic signatures during transit of the Sun's far hemisphere requires attention to two major component tasks:

(*Task 1:)* calibration of the dependence of the sensitivity of $S$ to location in the far hemisphere, and

(*Task 2:)* an assessment of the uncertainty in $S$ imposed by random noise.

Lacking an account of the first, an active region moving from a location in which the diagnostic is less sensitive to one in which it is more sensitive will errantly appear to grow in strength, $S$. Nevertheless, it is possible to assess the *feasibility* of Task 2 without undertaking either task as is required for a finished production line. This is the object of the discussion that follows.

The analysis we now describe was applied to the strengths, $S$, of the seismic signatures of FSSSM large-active-region signatures during Intervals 1 and 2. This dataset is posted on `http://www.cora.nwra.com/~lindsey/Seismic_Sigs.txt`. The basic data product

computed by the FSSSM is a map of the far hemisphere representing seismic correlations between waves converging to focal points in the far hemisphere and their returning echos integrated over 24-hour periods. These "24-hour snapshots," are produced at 12-hour intervals.

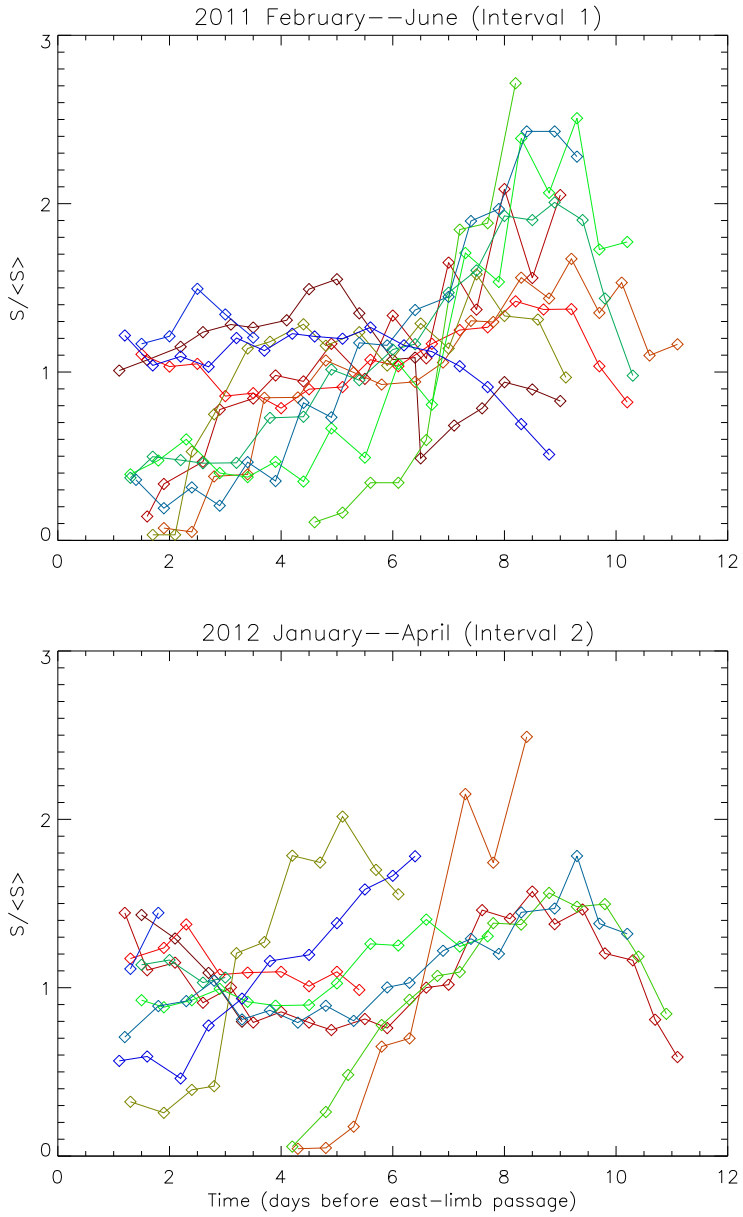


Figure 1. Seismic-strength profiles of the 22 seismic signatures of the active regions in Intervals 1 and 2 of this study. Time is represented in days *before* east-limb passage. Each profile is normalized to a mean value of unity. Hence, time proceeds from the right of the plot to the left, the east-limb passage being at the left ordinate axis. The profile of the first seismic signature, that of FS-2011-002, first appearing in the far hemisphere on 2011-02-15 and rotating into the near hemisphere on 2011-02-25, is plotted in magenta. Plots of subsequently appearing signatures are colored in the order of the colors of the rainbow, ending with FS-2012-010 (2012-04-08 to 2012-04-10) in bright blue.

The most useful data product for a broad range of applications is 5-day means of the 24-hour snapshots, for a signal-to-noise that is greatly improved over that of the 24-hour snapshots, even if at some possible expense in temporal resolution.*

Figure 1 shows the trajectories of the 12 FSSSM large-active-region seismic signatures in Interval 1 (top frame) and the 10 others in Interval 2 (bottom) during the last 11 days of their transit across the far hemisphere. These time series are truncated at approximately 36 hours before passage across the east limb (left edge of Figure) where partial disappearance of the signature from the seismic map causes an apparent decline in the seismic signature. Because the point is to gauge the ability of the diagnostic to distinguish between the kinds of growth rates individual active regions can exhibit irrespective of their initial or mean strengths, these profiles are normalized to a mean of unity. This condenses the strength profiles into a much narrower ordinate range than shown by the absolute strength profiles, accentuating the growth characters of the regions over the range in mean strength.

The trajectories plotted in Figure 1 show a general tendency of seismic signatures to appear somewhat more precipitously than their subsequent decay. This tendency of precipitous rise followed by a slower, roughly monotonic decay strongly reflects both their EUV-intensity and magnetic-flux counterparts (Ugarte-Urra et al 2015). There are, nevertheless, major and frequent exceptions to this tendency: Some of the individual seismic signatures plotted in Figure 1 decay by an order of magnitude over their far-side transit, while others experience persistent growth over days, and sometimes growth spurts by a factor of up to two.

A quantitative analysis of the data plotted in Figure 1 indicates that the various growth and decay attributes of seismic signatures with strengths typical of those recognized by the FSSSM large-active-region discriminator, i.e., $\sim$500 $\mu$hem radian, based on its evolution over the previous five days, can be forecast five days into the future with a diagnostic uncertainty of $\sim$150 $\mu$hem radian. `http://www.cora.nwra.com/~lindsey/growth_diag.pdf`. This uncertainty is less than typical growths and decays of FSSSM large active regions over a 5-day period, which can change by up to an order of magnitude in some instances.

## 3. Relationship Between Seismic Signature Strength and their EUV-Intensities and Magnetic Counterparts

The previous section focused on seismic-signature behavior. This section addresses the underlying meaning in that behavior, and what it can tell us about solar activity that can be of use to space-weather forecasting.

* For purposes of gauging growth rates, any loss of temporal discrimination resulting from averaging multiple maps together for each day in place of a single snapshot is only apparent. The way the 5-day means are computed is invertible; thus, the 24-hour snapshots can be reconstucted from the 5-day means with the growth rates preserved.

As enumerated in the third paragraph of §1, the focus of the Phase-1 effort is the relationship between seismic signatures and (1) the EUV intensity, $J$, of the active regions signified and (2) the unsigned magnetic flux, $\Phi$, of the same. We will begin with an assessment of the first.

*3.1 Seismic Signatures and EUV Sources*

For this part of the investigation, we examine the STEREO HeI 304 Å sources in the neighborhoods of all of the 22 seismic FSSSM large active regions in Intervals 1 and 2. As mentioned before, a list of the locations and strengths of these regions is conveniently posted on `http://www.cora.nwra.com/~lindsey/Seismic_Sigs.txt`, including NOAA designations of the active regions that eventually rotated into direct view from Earth. For each of the FSSSM large-active-region seismic signatures in Intervals 1 and 2, we examine a concurrent STEREO HeI 304 Å intensity map and identify a corresponding conspicuous cospatial EUV source. Figure 2 shows an example in the HeI 304 Å intensity map of 2011-02-21.0 (top frame), closely concurrent with the far-side seismic map (middle frame, amber) and the corresponding FSSSM large-active-region identification map (bottom frame). An elliptical region, $\mathcal{E}$, is fashioned to encompass the preponderance of the excess EUV emission (top frame, interior of red closed curve), over which the HeI 304 Å emission in excess of that of the mean quiet Sun—normalized to unity for the quiet Sun—was integrated. This defines, for this discussion, the "excess HeI 304 Å intensity," $\Delta J$ of $\mathcal{E}$. This is done for each 12-hour sample of the FSSSM large-active-region seismic signatures a long as it remains extant in the FSSSM tabulation.

Figure 3 show a scatter plot of the resulting integrated "HeI 304 Å intensities," $\Delta J$ (ordinate), against corresponding seismic strengths, $S$ (abscissa), for all of the FSSSM large-active-region seismic signatures in Intervals 1 and 2. The best power-law fit to these data points is a square-root relationship, plotted in magenta, with an ordinate scatter of $\pm 0.026$ hem over all of the data points in the plot, i.e., of the same order as $\Delta J$ itself. This is similar to the scatter in the relationship between magnetic flux and excess EUV intensity as observed from HMI line-of-sight magnetograms and AIA. This scatter appears to result from significantly different mechanisms that are important to each. For example, while it is well known that flares can drive detectable transient seismic emissions during their impulsive phases, they have practically no effect on seismic-scattering phase shifts, the basis of far-side seismic signatures. But, flares can release enormous amounts of EUV radiation.

The trajectories of FS-2011-012 (later to be designated NOAA AR 11236, red curve) and FS-2012-002 (later to be designated NOAA ARs 11236 and 11423, green curve) are plotted as examples of how differently different active regions can evolve both seismically and in EUV intensity. The latter decreases in both and then increases in seismic strength, while the former precipitously increases in seismic strength while mostly decreasing in EUV intensity.

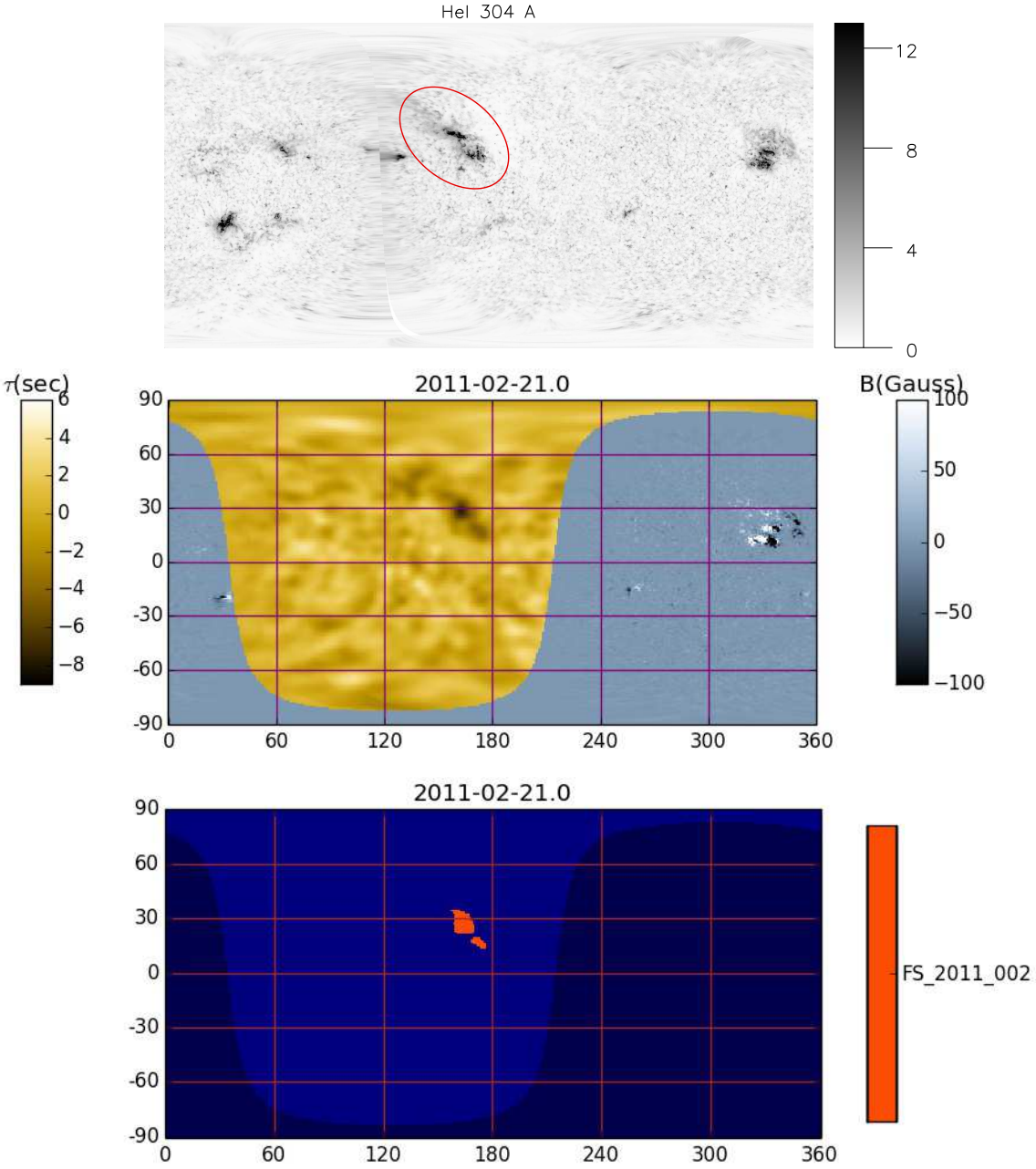


Figure 2. STEREO B map of the Sun in HeI 304 Å on 2011-02-21.1 is shown (top frame) with the cotemporal/cospatial composite seismic (amber)/magnetic (blue-gray) map of the Sun (middle frame) and FSSSM Large-Active-Region Identification Map (bottom frame). The HeI 304 Å intensity (top frame) is normalized to unity for the mean quiet Sun. The red ellipse in the top frame surrounds the region designated FS-2011-002 in the FSSSM Large Active-Region Identification map. The HeI 304 Å intensity in excess of the mean quiet Sun is integrated over the interior of this ellipse as an indicator of the EUV intensity plotted in the ordinate direction in Figure 3. The seismic signature is integrated over the two orange regions in the FSSSM Large-Active-Region Identification map (bottom frame) as an indicator of the seismic strength of the region. This is plotted in Figure 3 (bright red locus) with the seismic strength represented as the abscissa value.

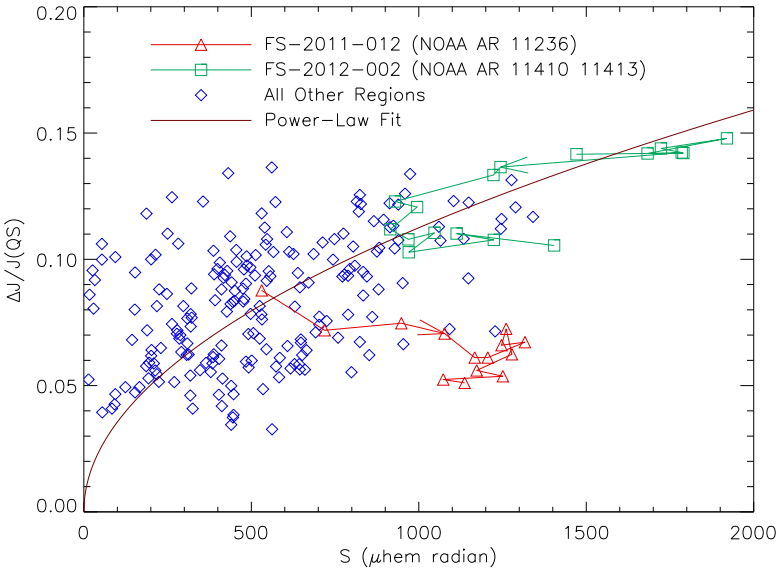


Figure 3. Plot of HeI 304-Å intensities, $\Delta J$ (ordinate), in excess of the mean quiet-Sun intensity, $J(\mathrm{QS})$, normalized to $J(\mathrm{QS})$, for FSSSM large active regions in Intervals 1 and 2 versus respective strengths of the helioseismic signatures (abscissa). The red data points (triangles) and connecting line segments show the trajectory of FS-2011-012 (subsequently NOAA AR 11236), an anomalous region whose EUV intensity decreased to ∼57% of its maximum value as its seismic signature more than doubled from 2011-06-05 to 14. The green locus shows the trajectory of the region with the strongest seismic signature, FS-2012-002, in Intervals 1 and 2 from its first appearance in the far hemisphere, on 2012-01-14.5, to 2012-01-027.0, when it rotated into direct view from Earth. All of the other data points (open blue diamonds) represent the other 10 active regions in Interval 1 and other 9 in Interval 2. The magenta curve is a fit of a square-root profile to the blue and green data points. *Note*: Because of the proximity of FS-2012-004 to FS-2012-005, the former is incorporated into the latter as a single set of data points in this analysis to circumvent the need for subjective judgements as to which components of the EUV emission are to be associated with the individual seismic signatures.

In summary, then, EUV emissivity is highly influenced by magnetic processes in the corona that have little effect on seismic signatures. This probably explains the significant spread in the correlation between helioseismic signatures and EUV intensity. There is, nevertheless a strong correlation between helioseismic signatures and EUV intensity, to the degree that a strong helioseismic signature will generally be a reliable indicator of sufficient EUV intensity that space-weather forecasters would want to know about it.

### *3.2 Relationship Between Seismic-Signature Strength and Magnetic Flux*

To examine the relationship between helioseismic signatures and magnetic properties of the active regions that elicit them requires that we compare the helioseismic signature during transit of the far hemisphere with magnetic observations made sometime later, when the region in question has rotated into direct view from Earth. This entails a delay of several days between the helioseismic and magnetic observations. For the purposes of

such a comparison, CoI Leka has compiled unsigned magnetic flux estimates, $\Phi$, of some of the FSSSM large active regions:

$$\Phi \equiv \int_{\mathcal{R}} |\mathbf{B} \cdot \hat{\mathbf{r}}| \, d^2a, \tag{6}$$

where $\mathbf{B}$ represents the vector magnetic induction, $\hat{\mathbf{r}}$ represents the local unit-outward-radial vector, the integral being applied to HMI vector-magnetic observations of active regions designated by NOAA/SWPC observations from 1 to 3 days subsequent to crossing of the Sun's eastern limb. Analysis of these results is ongoing.

As a template for the more careful analysis, and a powerful control taking advantage of the HMI line-of-sight magnetograms covering the full near hemisphere, we have run a parallel analysis working with one of several popular facsimilies for $\Phi$: This is literally the flux, $\Phi_{\rm los}$, of just the line-of-sight component,

$$\mathbf{B}_{\rm los} = (\hat{\mathbf{B}} \cdot \hat{\mathbf{n}})\hat{\mathbf{n}}, \tag{7}$$

of $\mathbf{B}$, taken from HMI line-of-sight magnetograms, wherein $\hat{\mathbf{n}}$ is the local unit vector along the line of sight. Hence,

$$\begin{aligned} \Phi_{\rm los} &= \int_{\mathcal{R}} |\mathbf{B}_{\rm los} \cdot \hat{\mathbf{r}}| \, d^2a \\ &= \int_{\mathcal{R}} |(\mathbf{B} \cdot \hat{\mathbf{n}}) \, (\hat{\mathbf{n}} \cdot \hat{\mathbf{r}})| \, d^2a. \\ &= \int_{\mathcal{R}} |B_{\rm los}| \, (\hat{\mathbf{n}} \cdot \hat{\mathbf{r}}) \, d^2a \end{aligned} \tag{8}$$

We have identified all of the active regions that emerged into view from Earth at the locations of the FSSSM large-active-region seismic signatures identified by Stanford in Intervals 1 and 2, from HMI line-of-sight magnetograms, and computed $\Phi_{\rm los}$ from these as they passed through the meridian in the near hemisphere, seven days after their respective crossings of the Sun's eastern limb.[⊗] Figure 4 shows the results of this comparison, where the strengths of the active regions are taken 36 hours before they crossed the Sun's eastern limb.

[⊗] In equations (6), (7) and (8), $\mathcal{R}$ is the same elliptical region, $\mathcal{E}$ applied to the HeI 304 Å intensity maps (see top frame in Figure 2) for the ordinates plotted in Figure 3. Care was taken to secure that no significant newly emerged flux had infringed into these regions since limb crossing.

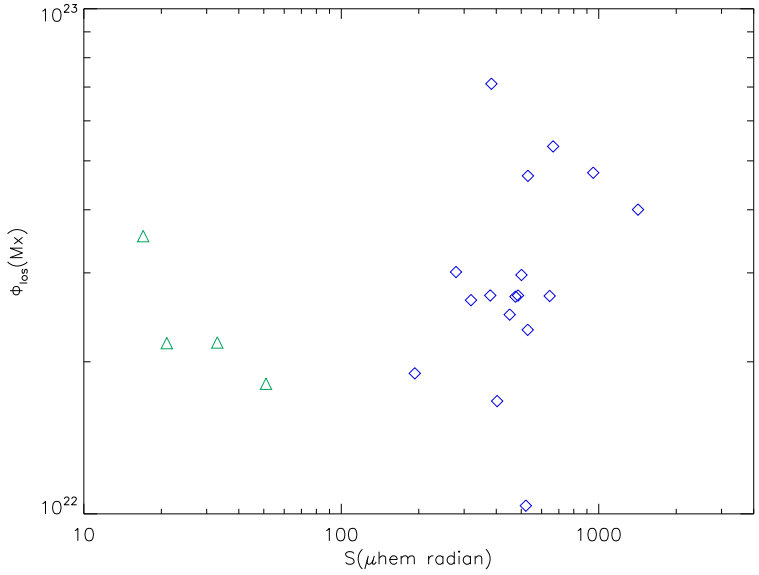


Figure 4. Line-of-sight component, $\Phi_{\rm los}$, of the magnetic flux, $\Phi$, of the FSSSM large active regions in Intervals 1 and 2 are plotted (abscissa) as they subsequently pass through the meridian in the Sun's near hemisphere against the strengths, $S$, (ordinate) of their helioseismic signatures ∼36 hours before they crossed the eastern solar limb and rotated into direct view from Earth. The points plotted in green represent the seismic signatures of FS-2011-007, FS-2011-008, FS-2011-010 and FS-2012-006, which had decayed to a small fraction of their maximal seismic strengths during their transit of the far hemisphere.

It is evident from Figure 4 that the helioseismic signature for two regions of approximately equal $\Phi_{\rm los}$ can be more than an order of magnitude different from each other. This is highlighted in Figure 4 by plotting in green points for which the seismic strength is less than 100 $\mu$hem radian, as opposed to blue for seismic strengths greather than 100 $\mu$hem radian. In fact, when we looked at the biographies of these points (which the FSSSM would never have been designated as large active regions had they never exceeded 100 $\mu$hem radian), it was conspicuous that the seismic signatures of all of these had once been very strong, and that, during their transit of the far hemisphere, they had decayed to a small fraction of their maximum strength, apparently while retaining a significant fraction of their original magnetic flux. Figure 5, then, shows the same plot, but with the seismic strength 36 hours before crossing of the eastern limb replaced by the maximum of the seismic strength—for all the regions—for the duration of their transit of far hemisphere.

This results in a much tighter relationship between the seismic strength and the line-of-sight component of the magnetic flux during meridian passage. The best power-law fit to this more compact clustering of points appears to be one for which $\Phi_{\rm los}$ increases with $S_m$ in proportion to its square root, as plotted in magenta in Figure 5.

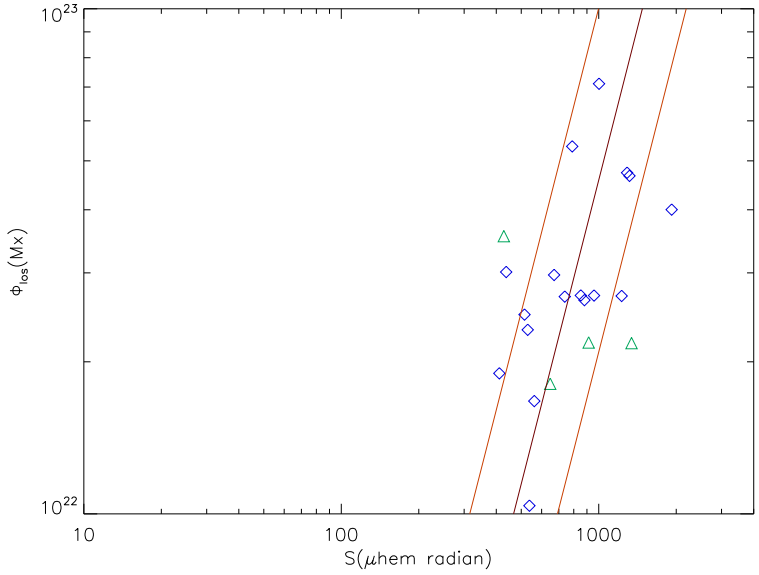


Figure 5. The line-of-sight magnetic fluxes plotted in Figure 4 are re-plotted here against the respective *maxima*, $S_{\max}$, of their helioseismic strengths, $S$, during their preceding transit of the Sun's far hemisphere. The best power-law fit to this clustering of points is that plotted in magenta, with $\Phi_{\rm los}$ in proportion to the square root of $S$. The orange lines on either side of the best fit mark the rms deviation of the data points from the fit. The orange curve to the right of the fit represents abscissa value $S_+$, i.e., 1.46 *times* the fit abscissa value; the orange curve on the left represents the the abscissa value $S_-$, i.e., the fit abscissa *divided* by 1.46.

## 4. Active-Region Seismic Signature Component Discrimination

At the outset of the project we had already developed some basic tools for the task of discriminating different components of active-region seismic signatures. Specifically, we implemented an initial version of our SSLW (Seismic Signal Landscape Watershed) algorithm (called SSLW1) that treats the seismic signature as a landscape and discriminates the different components on the basis of the different coastal watersheds for that landscape. Applying this algorithm to all of the seismic signatures in Intervals 1 and 2 gives results that are generally in line with intuition, but are overly sensitive to natural variability of the seismic signal. Relatively small, noise-level, variations in the neighborhoods or local maxima, saddlepoints, and "flatlands" cause watershed divisions that vary stochastically from one sample to the next. This complicates the identification of active-region components, especially when the farside field is complex, e.g., when active-region splitting and recombination events occur.

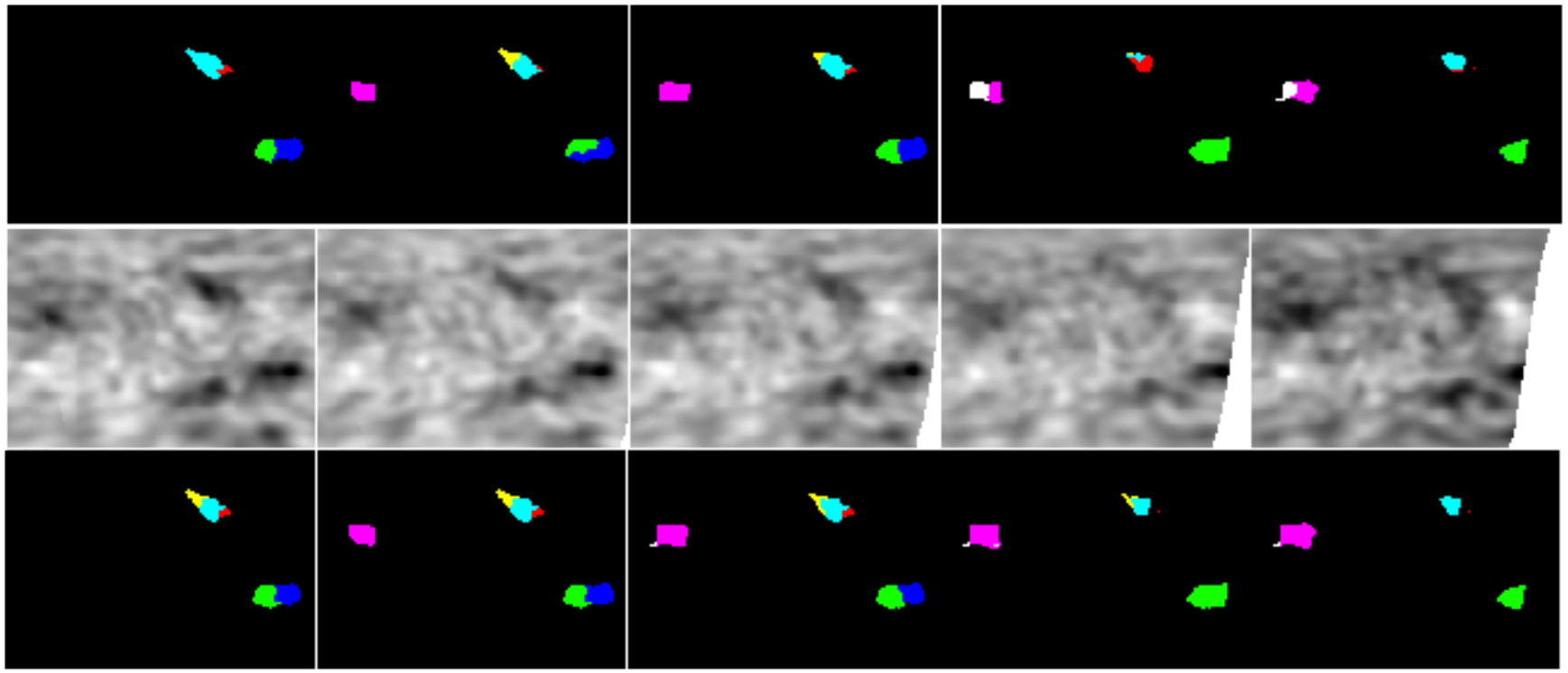

Figure 6: Results for two algorithms under development for discriminating active-region components (top and bottom rows) derived from a time sequence of farside seismic signals (middle row) for 20-22 March 2011. The top row shows results for the SSLW1 (Signal Signal Landscape Watershed 1) algorithm. The bottom row shows results for our TCLW1 (Threshold Contour Landscape Watershed 1) algorithm. While SSLW1 is sensitive to the large, natural variations in the seismic intensity (e.g., note the rapidly evolving component boundaries for each of the identified large active regions in the top row of images), TCLW1 is notably less sensitive (e.g., note the relatively more stable component boundaries in the bottom row of images). For this reason we anticipate TCLW1 will prove more reliable and consistent in successfully identifying active-region components when the seismic maps are complex. See discussion in the main text for a more detailed description. The images in each panel are separated by 12 hours.

We are exploring alternative and improved algorithms that reduce this sensitivity to the seismic signal. TCLW1 (for Threshold Contour Landscape Watershed 1) is one such algorithm. It develops a landscape based on the minimum distance between an interior point and the threshold contour that defines a large active region. TCLW1 then smooths the resulting landscape by applying a diffusion operation before the coastal watersheds are computed. This procedure exhibits significantly reduced sensitivity to the seismic signature variations, and instead tracks only the much smaller variations in the signature's defining threshold contour. Figure 6 demonstrates TCLW1's relatively greater stability compared to SSLW1 by simultaneously showing results obtained using both algorithms. While the SSLW1 results vary significantly over the 12-hour period between the images, the TCLW1 results are much more stable. Because of these results, we expect TCLW1 will lead to more reliable identification of evolving active-region components, especially when the seismic maps are complex. We will continue developing TCLW1, and we will apply it, SSLW1, and other algorithms we are investigating to the farside seismic data in Intervals 1 and 2 so that we may employ the most robust method for discriminating and identifying active-region components

## 5. Plans for Work in Period 3

*Repeat the Analysis of Magnetic Correlations with HMI Vector-Magnetograms.* The analysis described in §3.2 addresses the primary components of Tasks 3, 4 and 5. It was based on comparisons between helioseismic signatures of large active regions with the line-of-sight component of the magnetic flux derived from HIM line-of-sight magnetograms. A more accurate representation of the magnetic flux can be derived from the HMI vector magnetograms. This analysis has already begun, and will be completed in Period 3.

*Analyze the Long-Term Stability of Seismic Signatures of Activity in the Far Hemisphere.* This is Task 6 of the Project. It is partially covered by work described in Period 2, analyzing active regions in Intervals 1 (2011) and 2 (2012), as described in §3. This Task will be completed in Period 3 by comparing more recent seismic signatures, in 2015, with those in Intervals 1 and 2.

*Test Tools for Discrimination of Morphological Components of Seismic Signatures.* Basic tools for this undertaking, Task 2 of the project, were developed on schedule in Period 1, and were used to identify the domains of all of the seismic signatures in Intervals 1 and 2. However, these algorithms were subject to instabilities explained in §4 of this report, due to day-to-day noise-like variations in the seismic signatures. CoI Werne developed some further tools in a Period-2 extension of Task 2. Encouraging results of preliminary tests of these tools are shown in §4. More extensive tests, and probable adjustment of tool parameters will be done in Period 3.

*Technical Review Meeting and Final Report.* We will hold a meeting at NOAA/SWPC to review and discuss the results of this project in about the middle of the second month of Period 3. We will deliver the Final Report on the Project at the end of Period 3.

## 6. Findings and Recommendations

The results of the Project at the end of the Second Period are highly encouraging as to the facility of seismic monitoring of the Sun's far hemisphere to develop a data product with the following qualifications:

1. the ability to detect large active regions in the Sun's far hemisphere.
2. the facility of discriminate rapidly growing active regions from nominally decaying ones.
3. reliable applications in UV and EUV irradiance forecasting, quantifying EUV emissivities from individual large active regions in the far hemisphere to within a factor of about 2.
4. the ability to recognize new rapidly growing emerging magnetic flux in the Sun's far hemisphere.
5. the likely facility to quantify newly-emerged magnetic flux in the far hemisphere to within a factor of about 2.

Seismic monitoring of the Sun's far hemisphere appears to be encumbered by the following significant limitation: It is much less sensitive to solar activity than direct observations of the Sun in EUV, visible chromospheric lines, and probably even the visible continuum. Moreover, what seismic monitoring shows the best is by benefit of averaging of the seismic signature over some 120 hours, reducing its sensitivity to moderate quantities of magnetic flux that emerges only a day or two before crossing the Sun's eastern limb. This suggests that EUV or X-ray observations of the corona overlying the active-region band approaching the eastern limb from the far hemisphere would be a useful complement to seismic monitoring of the Sun's far hemisphere for applications in space-weather forecasting. In summary, then, seismic monitoring of the Sun's far hemisphere is no match for the powerful tools of optical observations in the visible, UV and X-ray spectrum. It is, nevertheless, a great deal better than what we will otherwise have in the third decade of the millennium once STEREO has lost its far-side vantage, is relatively economical, and is ideally adaptable to facilities such as SDO and GONG that are designed for a broad variety of other useful applications.

## 7. Table of Work Efforts

| | | | |
|---|---|---|---|
| Lindsey | PI | 120 hours | Tasks 1–4 |
| Braun | Co-I | 0 hours | Task 6 (N/A here) |
| Werne | Co-I | 12 hours | Tasks 2, 3 |
| Leka | Co-I | 36 hours | Tasks 2, 3 |
| Barnes | Co-I | 8 hours | Tasks 2, 3 |
| Hill | Co-I | 0 hours | Tasks 5–7 (N/A here) |

Co-Is Hill, Liewer, Zhao, Scherrer contributed considerable labor to this project free of charge.

## 8. References

Mihalas, D. 1978 *Stellar Atmospheres* W. H. Freeman & Co., London, p. 5.

Ugarte-Urra, I., Warren, H. P. & Hathaway, D. H. 2015 "Magnetic Flux Transport and the Long-Term Evolution of Solar Actie Regions," *Ap. J.* **815**, 90.